Discrete Nanocubes as Plasmonic Reporters of Molecular Chirality

Fang Lu,[†] Ye Tian,[†] Mingzhao Liu,[†] Dong Su,[†] Hui Zhang,[‡] Alexander O. Govorov,[‡] and Oleg Gang*,[†]

[†]Center for Functional Nanomaterials, Brookhaven National Laboratory, Upton, New York 11973, United States
[‡]Department of Physics and Astronomy, Ohio University, Athens, Ohio 45701, United States

S *Supporting Information*

ABSTRACT: One of the most intriguing structural properties, chirality, is often exhibited by organic and bio-organic molecular constructs. Chiral spectral signatures, typically appearing in the UV range for organic materials and known as circular dichroism (CD), are widely used to probe a molecular stereometry. Such probing has an increasingly broad importance for biomedical and pharmacological fields due to synthesis/separation/detection of homochiral species, biological role of chiral organization, and structural response to environmental conditions and enantiomeric drugs. Recent theoretical and experimental works demonstrated that the CD signal from chiral organic molecules could appear in the plasmonic (typically, visible) band when they coupled with plasmonic particles. However, the magnitude of this CD signal, induced by discrete nonchiral plasmonic particles, and its native molecular analog were found to be comparable. Here we show that shaped nonchiral nanoparticles, namely, gold/silver core/shell nanocubes, can act as plasmonic reporters of chirality for attached molecules by providing a giant, 2 orders of magnitude CD enhancement in a near-visible region. Through the experimental and theoretical comparison with nanoparticles of other shapes and materials, we demonstrate a uniqueness of silver nanocube geometry for the CD enhancement. The discovered phenomenon opens novel opportunities in ultrasensitive probing of chiral molecules and for novel optical nanomaterials based on the chiral elements.

KEYWORDS: *Silver nanocube, molecular chirality, circular dichroism, surface plasmon, DNA*
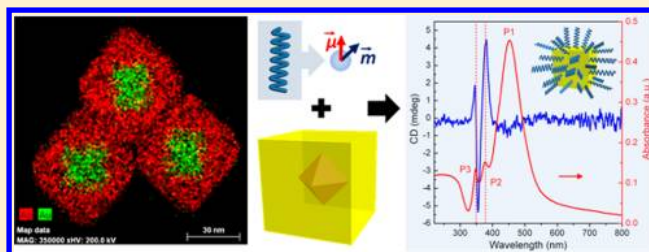
Molecular constructs often exhibit a chiral organization.[1] Chirality is also frequently observed in biomolecules due to the formation of secondary and tertiary structures, for example, helices of nucleic acids and proteins;[2] such structural organization is crucial for their proper biological functionality.[3] One of the well-established methods to probe chiral properties relies on the optical activity of chiral molecules due to their different optical absorption of left and right circularly polarized light. The method, known as circular dichroism (CD) spectroscopy, is widely utilized to examine the efficiency of synthetic organic chemical reaction and concentration of enantiomers, protein folding, and change of their conformational states due to physical and chemical stimuli, like radiation, temperature, pH, biochemical reactions, and drug interactions.[4,5] For organic molecules the CD signal is typically weak; thus, significant amounts of material at relatively high concentrations are required for detectable signals, which is frequently an impediment for a practical use. Moreover, the optical transitions in organic and biological molecules are normally in the ultraviolet (UV) region (150−300 nm).[2,4] When an achiral chromophore is placed to the vicinity of a chiral component, that is, the otherwise symmetric chromophore faces lower symmetry due to its environment, a conventional induced CD is observed. However, such an induced CD is usually at least 1 order of magnitude smaller than normal CD.[6] Possible probing of optical chirality beyond UV range ($\lambda > 300$ nm) is being actively sought after for a quantitative analysis and for using in pharmacology fields. For

nanoscale and micrometer-scale systems, the breaking of circular polarization symmetry further provides a promising way for the modulation and encoding of photon polarization states in nanophotonic devices and metamaterials,[7,8] for which novel fabrications of discrete and larger-scale chiral structures are required.[9−12]

Resent advancements in molecular sensing exploit the effects related to plasmon resonances. For example, vibration spectrum of single molecules, observed using surface enhanced Raman scattering (SERS), is related to the amplification of electromagnetic fields by plasmonic nanoparticles.[13,14] Also, plasmonic effects lead to the enhanced fluorescence emission of molecular dyes and quantum dots.[15,16] Recently, it was theoretically proposed that plasmonic nanostructures under particular conditions might enhance molecular CD signals by orders of magnitude as well as echo its optical signature from UV into plasmonic bands.[17,18] This novel plasmon-induced CD signals far away from the molecular electronic transition may emerge from a hybrid complex, plasmonic nanoparticle−chiral molecules, also known as "discrete chiral plasmonic nanoparticles". In such structure, a tiny difference between left- and right-handed refractive indices (n_+ and n_-) slightly shifts the plasmon resonances, which can be detected by CD spectros-

copy with a high sensitivity. This effect is analogous to the dielectric sensing by localized surface plasmon resonance.[19] Such a realization, if successful, can pave a road for novel biological, pharmaceutical, and synthetic applications. Moreover, a chiral optical response of nonchiral plasmonic elements functionalized with organic molecules can be potentially used in the nanophotonics field. However, to date only a limited number of experimental works have manifested the existence of surface plasmon (SP)-induced CD resonance from discrete chiral plasmonic nanoparticles[20] or planar nanofabricated chiral structures.[21] Comparatively, CD resonance in the SP region is often observed from the congregate systems of plasmonic nanoparticles such as clusters, aggregates, and arrays.[12,22−28] Recently, the amplification of the chiral activity was observed in the two-dimensional arrays of gold particles, and its influence on the molecule-to-surface separation was investigated.[27] In the current studies we report an experimental scheme, previously not considered theoretically, in which discrete silver nanocubes act as plasmonic supports for chiral molecules (DNA) and induce a giant CD signal in the silver plasmon band. For discrete nonchiral nanocubes, we observed about 2 orders of magnitude enhancement of chiroptical activity per molecule in the near-visible range relative to the DNA native CD signal in the UV region. Through the detailed investigations of nanocubes and particles of other shapes we show that the effect originates in the exciton−plasmon interactions. We also found that a molecular orientation relative to a particle surface is critical for the observed strong CD enhancement.

In the search for a much-anticipated plasmonic "amplifier" of chiroptical activity we have considered Ag, whose localized surface plasmon resonances (LSPR) and thus their interaction with light can be fine-tailored across a broad spectral range, from 300 to 1200 nm, by sculpturing nanoparticle size and shape.[29] Recent advances in the solution-phase synthesis of Ag nanoparticles allow for the controllable formation of various shapes (spheres, cubes, octahedrons, and plates, etc.) by manipulating the growth of crystalline facets via facet-capping agents (surfactants).[30−32] In comparison, LSPR of Au nanoparticles, another typical plasmonic material, is limited to wavelengths longer than 500 nm due to the d−sp interband transitions. LSPR of Ag also enjoys a significantly lower loss,[33] which leads to narrower spectral lines and a more detectable spectral fine structure.[34]

In Figure 1 illustrated our design strategy: we have developed method for synthesizing Au/Ag core−shell nanocube (NC) via a seed-mediated approach and attaching DNA molecules to NC. We choose single stranded (ss) and double stranded (ds) DNAs as molecular objects with inherent CD signatures in UV region as model systems to study plasmonic effects for molecular constructs ssDNA with its chiral sub-blocks (nucleotides) and dsDNA with overall chiral secondary/tertiary structure (DNA duplex), respectively.

The as-synthesized nanocubes are subsequently functionalized with 30- and 50-base long thiol-modified ssDNA (see Supporting Information). Scanning electron microscopy (SEM) images of ssDNA-functionalized nanocubes (NC) indicate 42 ± 2 nm edge length of the resultant nanocubes (Figure 1b,c). A high size and shape monodispersity of NC results in formation of ordered arrays (Figure 1b). The DNA-functionalized nanocubes show relatively sharp profiles of edges and corners (Figure S1a). The internal structure of NC with its Ag shell and ∼20 nm Au octahedral core is revealed with transmission electron microscopy (TEM) and scanning TEM
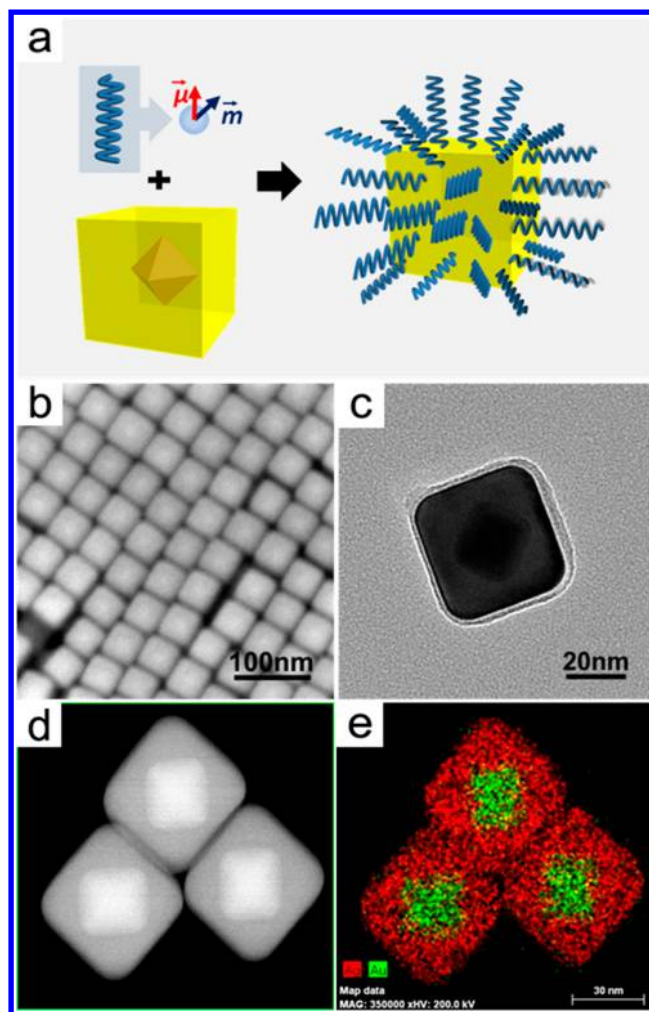

Figure 1. Plasmonic nanoparticle with chiroptical activity, based on silver nanocube and DNA. (a) The design of "individual plasmonic chiral nanoparticle" using a gold/silver (Au/Ag) core−shell nanocube (namely, Ag NC) surface-functionalized with chiroptical molecules (e.g. DNA), theoretically expected to exhibit a plasmon-induced circular dichroism (CD) response. Structural characterizations of single-strand (ss) DNA-functionalized Ag NCs (b−e). (b) Low-magnification scanning electron microscopy (SEM) and (c) transmission electron microscopy (TEM) images show size and shape uniformity of nanocubes with edge length of 42 ± 2 nm. (d and e) Scanning transmission electron microscopy (STEM) and the corresponding energy dispersive X-ray (EDX) mapping images demonstrate that the nanocube is made of an octahedral Au core embedded with thick cubic shell of Ag.

(Figure 1c−d, S1b). The corresponding energy dispersive X-ray (EDX) (Figure 1e) mapping further confirms that an octahedral gold core is embedded in NC, with >8 nm thick shell of silver. Since the spectral properties of the nanocube are primarily determined by the thick Ag shell as indicated by numerical simulations (Supporting Information), we will refer it as Ag NC in the following text. The DNA-functionalized Ag NCs are stable and well-dispersed in the solution without spontaneous aggregation, as shown by dynamic light scattering (DLS) measurements (Figure S2).

Figure 2a illustrates typical intrinsic optical extinction features from two individual components of the DNA-NC complex, ssDNA and Ag NC, respectively. The ssDNA shows one characteristic UV peak at 264 nm. Prior to DNA
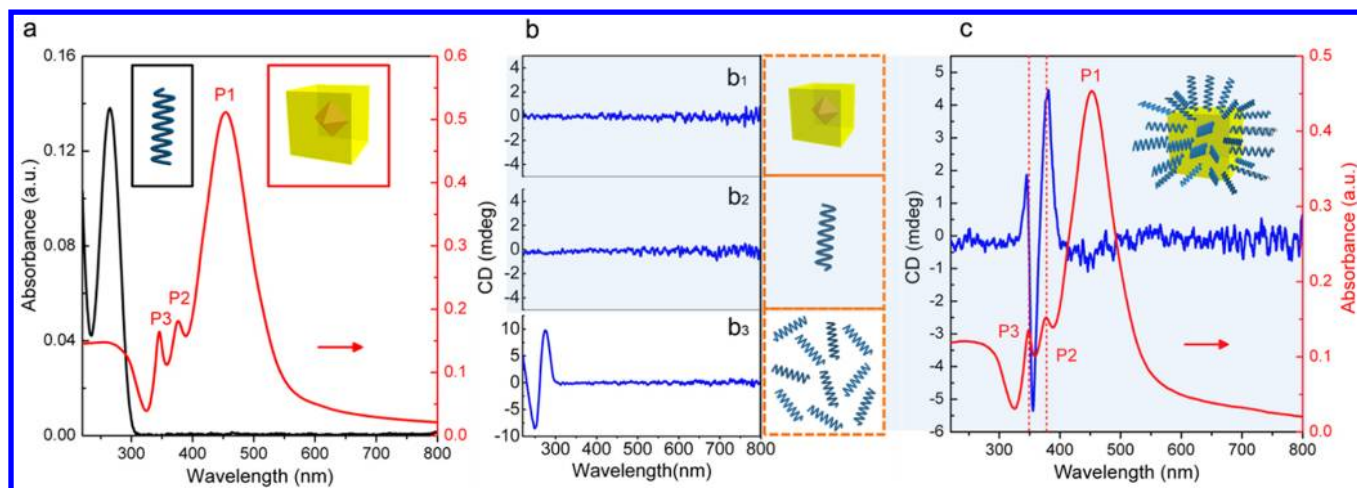
Figure 2. Optical responses of chiroptical ssDNA, non-chiral Ag NCs, and plasmonic chiroptical DNA-functionalized Ag NCs. a. UV−vis absorption spectra taken from two individual components of ssDNA-functionalized Ag NCs, ssDNA (illustration in a black frame), and virgin Ag NC (illustration in a red frame), respectively. The ssDNA strands (black curve) show one characteristic UV peak at 264 nm, and the virgin silver nanocubes (red curve) show three characteristic peaks at 452 nm (P1), 378 nm (P2), and 349 nm (P3), respectively. (b) The CD spectra were recorded from the virgin Ag NCs of 0.18nM (b_1), ssDNA of 0.1 μM (b_2), and 20 μM (b_3). No CD signal in b_1 is observed from the virgin nonchiral Ag NCs without DNA modification (framed illustration beside b_1). Due to the detector resolution limitation of instrument, natural chirality from little amount of DNA at 0.1 μM concentration (framed illustration beside b_2) cannot be presented in the CD spectrum of b_2. Observable CD signal from chiral ssDNA requires much more strands (framed illustration beside b_3). A thick specimen of ssDNA (20 μM) exhibits the characteristic bisignated CD peaks with maxima at 249 and 275 nm, respectively, in the spectrum of b_3. (c) UV−vis absorption and CD spectra of ssDNA-functionalized Ag NCs. The Ag NCs functionalized with ssDNA (red curve) show similar absorption features as the virgin ones do (red curve in b_1). However, the CD spectrum recorded from 0.18 nM NCs in 10 mM phosphate buffer (PB) (blue curve) exhibits novel features different from the spectral plateau of virgin Ag NCs: two positive Cotton effects are observed at 345 nm and 378 nm, respectively, together with a negative Cotton effect at 355 nm; the positive peak at 378 nm and another negative-Cotton-effect-induced split peak centered at 350 nm correspond well to two plasmonic resonance peaks of Ag NCs (P2 and P3). An enhancement factor (A_{CD}) of 85−103 is achieved from the ssDNA of 0.088−0.106 μM that are grafted onto the Ag NCs of 0.18 nM due to the plasmon-induced CD resonance mechanism.

functionalization, virgin Ag NCs show three characteristic peaks: a major one at 452 nm (P1, Mode 1) and two shoulder peaks at 378 nm (P2, Mode 2) and 349 nm (P3, Mode 3), each of which corresponds to a different LSPR modes. The electronic transition of ssDNA is clearly off the LSPR frequencies of Ag NCs. Our CD measurements (using Jasco J-815 instrument) are then performed for three solutions containing only virgin Ag NCs of 0.18 nM and only ssDNA of two different concentrations, 0.1 μM and 20 μM, respectively. No CD signal is observed for the virgin Ag NCs without DNA functionalization, which is expected due to the absence of chirality (Figure 2b_1). On the other hand, due to the sensitivity limitation of the instrument, natural chirality from a trace amount of ssDNA at 0.1 μM concentration is not observable in their CD spectrum (Figure 2b_2). Observable CD signal from chiral ssDNA requires a significantly larger concentration. Accordingly, as shown in Figure 2b_3, solution containing a two-hundred-fold higher concentration (20 μM) of ssDNA exhibits the characteristic bisignated CD peaks with maxima at 249 and 275 nm, respectively, which falls into the UV region (100−300 nm) and far from the typical plasmon resonance region of the Au and Ag nanoparticles (300−800 nm).[2] Recent theoretical work suggested that plasmon-induced CD resonance features can be activated when a nonchiral plasmonic nanoparticle is surrounded by chiral molecules.[17,18,35]

While there are a variety of methods to attach DNA to gold and selected semiconductor nanoparticles,[36−40] the functionalization of Ag nanoparticles with DNA has proven a challenge owing to the inherent lower binding energy of thiol groups to Ag[41,42] and the blocking of Ag surface by facet-capping surfactants required for synthesis, such as poly-

(vinylpyrrolidone) (PVP).[30−32] That is, the stubborn surfactant layer usually has strong affinity to the Ag surface and obstructs DNA from penetrating through and anchoring to particle surfaces in the functionalization process. Herein, we develop a seed-mediated method to synthesize monodisperse Ag NCs using cetylpyridinium chloride (CPC) as shape-controlling surfactant, which is known from our previous work as easily removable.[43] Effective DNA functionalization of Ag NCs is achieved through a combination of particle purification and incubation with DNA (Supporting Information). The DNA-NC complexes in a low ionic-strength solution (e.g., 10 mM phosphate buffer) would have dandelion-like morphologies wherein electrostatic repulsive DNAs will tend to arrange radially around the nanocube (a scheme in Figure 2c), which is also known as charged polymer brushes.[44] As shown in Figure 2c, DNA-functionalization has a negligible effect on the optical absorption profiles of the Ag NCs.

Remarkably, the ssDNA-functionalized NCs exhibit novel CD bands (Figure 2c) falling into Ag plasmon region (>300 nm), while virgin silver nanocubes at the same concentration exhibit no CD signal. Two positive Cotton effect peaks are respectively observed at 345 and 378 nm, together with a negative Cotton effect peak at 355 nm, being different from the CD spectra of both pure DNA and virgin NC. The positive signal at 378 nm and another negative-Cotton-effect-induced split peak centered at 350 nm are well aligned to two of the absorption bands of Ag NCs (Modes 2 and 3), implying that the CD signals are plasmon-induced. Due to the low amount of DNA in solution, the native CD signature of ssDNA around 240−280 nm is below our detection limit and absent from the CD spectrum.

Table 1. Comparison on CD Enhancement Factors, A_{CD}, from Different Nanoparticles Functionalized with 30 ssDNA^a

material/shape/size	Au sphere 10 nm (diameter)	Au sphere 45 nm (diameter)	Au cube 45 nm (edge length)	Au octahedron 45 nm (edge length)	Ag sphere 20 nm (diameter)	Ag sphere 40 nm (diameter)	Ag cube 42 nm (edge length)
enhancement factor (A_{CD})	N/A	N/A	N/A	N/A	1.6	N/A	85−103

^{a}N/A indicates that no plasmon-induced CD signal was observed at the measured concentrations (see Supporting Information).

Indeed, we estimate the 0.18 nM Ag NCs solution contains about 0.088−0.106 μM of 30-base ssDNA molecules that are all bound to the nanocube surfaces (see Supporting Information for the Ag NC optical extinction coefficient), which is beyond the sensitivity level of conventional detection using a conventional CD measurement with our modern instrument. Intriguingly, an intense CD signal up to 4.46 mdeg at 378 nm represents a significant enhancement of the CD response of the chiral ssDNA. We define a CD enhancement factor as $A_{CD} = (CD(\lambda_{plasmon})/CD_0(\lambda_{UV}))$, where $CD_0(\lambda_{UV})$ and $CD(\lambda_{plasmon})$ are the CD signals of freely dispersed DNAs and DNA-NC complexes respectively taken at the corresponding wavelengths of molecule electronic transition λ_{UV} and plasmon resonance $\lambda_{plasmon}$ and are normalized by DNA concentrations. Considering the detected CD intensity (9.74 mdeg) of free ssDNA at 275 nm from a solution of 20 μM (Figure 2b$_3$), the average CD enhancement factor at 378 nm is estimated from multiple measurements of various experimental batches as 85−103. This large CD enhancement factor is unexpected and is remarkable in its own right. The observed chiroptical activity can be represented by the anisotropy factor, g-factor ($g = (\Delta\varepsilon/\varepsilon)$, where $\Delta\varepsilon$ and ε are the molar circular dichroism and molar extinction, respectively), which for our DNA-NC system is equal to 0.0044. This magnitude of g-factor is significantly larger than previously the observed values for small-metal nanospheres, with SP-CD only registering below 0.001.[28] In fact, according to present theory on plasmon-induced CD, the signal for discrete nanoparticles is comparable in a magnitude to a native CD signal of molecular species. However, in our case, intense plasmon-induced CD signal is detected when the intrinsic DNA signal is too weak to detect, deeming it an *all-new phenomenon*. The magnitude of the plasmon-induced CD strongly depends on the composition and geometry of nanoparticles supporting the chiral molecules. As summarized in Table 1, our experiments show that other DNA-metal complexes including Au nanocubes, nanospheres, and nano-octahedron fail to exhibit detectable CD signal (Figure S3a−f), while small-sized Ag nanospheres (Figure S4) only show a few-times enhancement, which is comparable to the previously reported values.[17,20,45] In fact, only Ag NCs produce strong plasmon-induced CD in our study. The evident plasmon-induced CD response is also observed from the Ag NCs functionalized with 50 base ssDNA (Figure S3g). We note that particle curvature plays certain role in the density of grafted chains and, consequently, in the chain configurations and orientations.[46,47] The contribution of this factor calls for new theoretical studies bridging optical and polymeric effects.

In Figure 3A and B, we plot the CD enhancement factors, A_{CD}, against their respective LSPR spectra for the DNA-conjugated Ag NC, Au NC, and Ag spheres with diameters 20 and 40 nm. The electric field enhancement profiles shown in Figure 3 ($P = |\vec{E}|^2/|\vec{E}_0|^2$, where $|\vec{E}|$ and $|\vec{E}_0|$ are respectively the actual and incident electric field amplitudes) were calculated by the discrete dipole approximation (DDA) method[48] for the three LSPR modes of the Ag NC and for the single LSPR mode
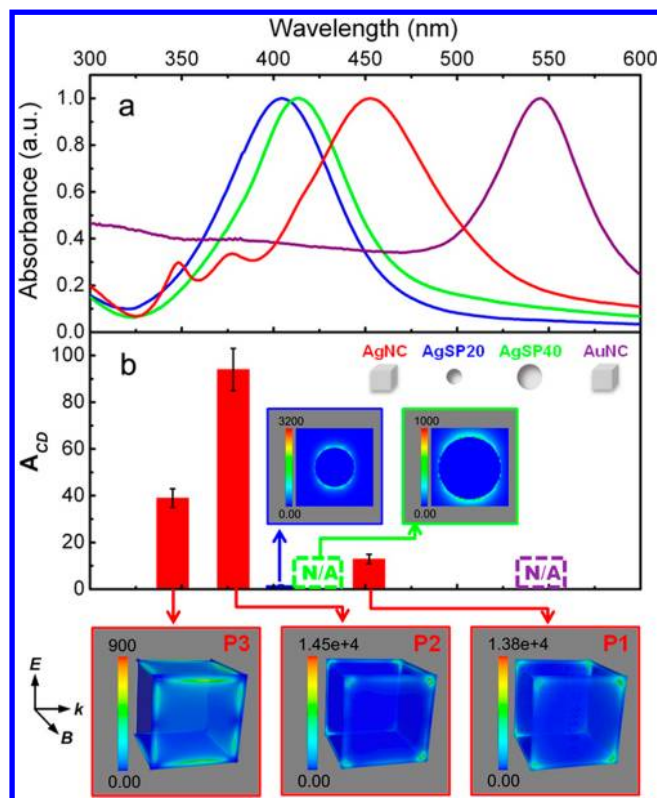

Figure 3. Comparison of optical resonance enhancement from DNA-functionalized nanoparticles (NPs). (a) The normalized UV−vis absorption spectra and (b) the CD enhancement factor (A_{CD}) associated with SPR peaks in spectra in a from different NPs. The NPs figurations are simplified to be the pencil sketches shown in the top-right inset of b; different NP objects are denoted by the caption color of the pencil sketches, i.e., red (curve/column/frame) for 42 nm edge Ag NC, blue for 20 nm diameter Ag sphere (AgSP20), green for 40 nm diameter Ag sphere (AgSP40), and purple for 45 nm-edge Au NC, respectively. The A_{CD} values of Ag NC are 13 ± 2 for P1, 94 ± 9 for P2, and 39 ± 4 for P3; AgSP20 is of 1.6 ± 0.2 for the 404 nm SPR peak; no enhancement is observed from AgSP40 and Au NC. The gray-background profiles in the colored frames are the calculated electric field enhancement $P = |\vec{E}|^2/|\vec{E}_0|^2$ at the Ag surface for the respective resonance modes, corresponding to SPR peaks shown in UV−vis absorption spectra from different Ag objects (see also Supporting Information for the more spectra and calculation details).

of the Ag spheres (see also the description of numerical calculations in Supporting Information and Figure S5−S7). The Ag spheres show $P \sim 10^3$, while the Ag NC exhibits a significantly larger electric field enhancement of up to ~10^4 times. Physically, shaped nanoparticle bearing sharp geometrical features enjoys higher P in its vicinity due to the lightning rod effect, which is highly favorable for a large CD enhancement according to theoretical considerations. However, by comparing the plasmonic field enhancement P and the CD enhancement A_{CD}, we note that their correlation is less straightforward than what the present theory suggests. For

instance, we note that A_{CD} at Mode 1 is much weaker than the other two modes of Ag NC, despite the mode has the largest local field enhancement ($P > 10^4$). On the other hand, $A_{CD} \sim 40$ is observed for Mode 3 for which $P < 10^3$. Finally, spherical Ag nanoparticles, diameters 20 nm and 40 nm, have comparable field enhancement as Mode 3 ($P \sim 10^3$) at their dipolar LSPRs (404 and 415 nm) but show either significantly low or no plasmon-induced CD enhancement at all, respectively (Figure 3). Although we point out that a distribution of DNA molecules on a nanocube surface can contribute to the observed effect: a larger number of DNA molecules is located at cube edges (Modes 2 and 3) than at apexes (Mode 1), this difference alone cannot be responsible for the observed strong CD enhancement. Furthermore, while Modes 2 (378 nm) and 3 (349 nm) are closer to the DNA electronic transition (264 nm) than Mode 1 (452 nm), the difference between n_+ and n_- would be only few times larger for Mode 2 and Mode 3 than Mode 1 (the optical rotatory dispersion, ORD, signal at frequency ω is proportional to $(\omega_0 - \omega)^{-1}$, where $\omega_0 > \omega$ is the molecular electronic transition frequency). Considering all of these findings and that the present theory is developed for spherical plasmonic nanoparticles with one single resonance, we believe that we have entered a new multimode regime of plasmon-induced CD. A more comprehensive theory, covering the geometry of plasmonic nanoparticles and the corresponding multiple resonances, is much needed.

The orientation of attached molecules is predicted to be crucial for the plasmon induced CD enhancement.[17,18,35] The strongest plasmonic CD appears typically for molecular dipoles perpendicular to a nanoparticle surface, when the strongest exciton−plasmon interaction is experienced. Thus, chiral molecules, randomly oriented to the plasmonic surface, may not be able to induce a significant plasmonic CD. We probe the effect molecular alignment on A_{CD} for our experimental system by varying the solution ionic strength, which determines the rigidity of ssDNA. As illustrated on a scheme in Figure 4a, DNAs on cube surface are reasonably aligned perpendicular to a surface at low/no salt conditions because of electrostatic repulsion of neighboring backbone units within the polyelec-trolyte chain and between chains.[44,49] A salt concentration increase reduces a persistence of ssDNA length, due to the electrostatic screening; thus, leading to a deterioration of chains alignment and more pronounced coiling, which, in turn, affects the orientation of chiral nucliotides. Our measurements, Figure 4b and c actually show that plasmon-induced CD signal of DNA-functionalized nanocubes fades down gradually when salt is added: the CD peak intensity at 378 nm decreases from 4.4 mdeg down to 0.2 mdeg with the corresponding ionic strength increase from 0 (deionized water) to 0.16 M (0.1 M phosphate buffer saline). We point out that the weakening of chiroptical activity due to the etching on silver NC corners and edges has been ruled out, as shown by NC stability in salt environments in our control experiments (Figure S9). At the same time, no change in the spectral position of CD signal is observed. As a reference, pure DNA solution shows no obvious decline in CD signal with a salt concentration increase (Figure 3c); that is due to the averaging of CD signal from randomly oriented nucleotides, which are located either on different freely dispersed ssDNA molecules or within single coiled ssDNA.

The rigidity of flexible ssDNA drastically increases after hybridization with a complementary strand due to the formation of a double helix in which nucleotides are aligned. Such process, with about 50 times persistence length increase,
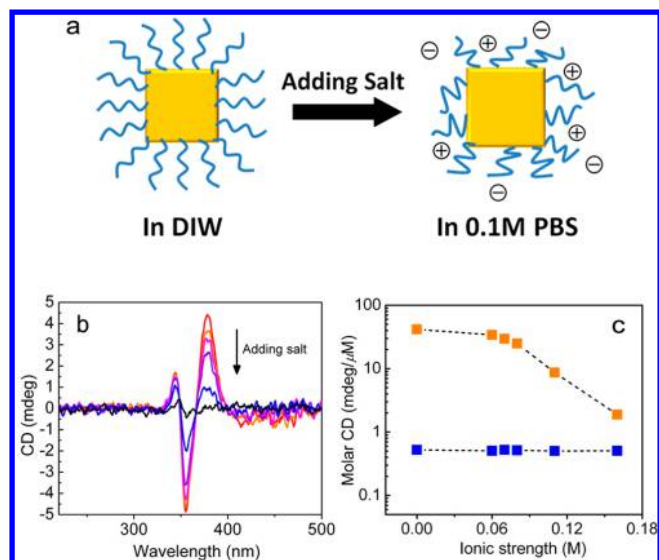

Figure 4. Dependence of plasmon-induced circular dichroism signal on a salt concentration. (a) Scheme illustrates a change of ssDNA alignment on a Ag cube surface after adding salt. (b) A salt-dependent CD spectra evolution of ssDNA-functionalized Ag NCs with the ionic strength increasing from 0 (deionized water, DIW) to 0.06 (10 mM PB), 0.07, 0.08, 0.11, and 0.16 M (0.1 M phosphate buffer saline, PBS) in the order indicated by a black arrow. (c) The comparison of the CD spectral dependence on NaCl concentration for ssDNA-functionalized Ag NCs (orange-squares-dash) and free ssDNA in the solution (blue-square-dash). CD signal intensities, monitored at 378 nm (NC-ssDNA) and at 264 nm (free ssDNA), were normalized by the corresponding DNA concentrations, 0.106 μM (NC-ssDNA) and 20 μM (free ssDNA). With the ionic strength increase, plasmon-induced CD signal of nanocubes fades down gradually, whereas no obvious decline in CD signal is observed from pure ssDNA system, which reveals different origins of the CD signal for two systems.

might restore the DNA orientation on a cube surface for plasmon-enhancement favoring alignment (Figure 5a). Indeed, our measurements demonstrate that the CD signal for ssDNA-functionalized nanocubes becomes undetectable at the ionic strength of 0.16 M. Nevertheless, upon the hybridization with complementary stranded ssDNA CD signal of dsDNA-functionalized nanocubes rises to the well-detectable magnitude of 2.1 mdeg at 376 nm (Figure 5b). Besides, in contrast to ssDNA, no significant decline in the magnitude of CD signal for dsDNA-NC complex was observed with a NaCl concentration increase, which is due to the high rigidity and stability of dsDNA at those salt concentrations. This observation also supports the discussed mechanism of reduction of CD signal for ssDNA due to the loss of the normal to surface alignment. Such high sensitivity of the plasmon-induced CD response to molecular orientation can be further used in the future applications for probing the alignment of chiral molecules at the surfaces and changes in their conformations.

In conclusion, new CD response is observed from the DNA-functionalized Ag NCs, in which the CD bands fall into the plasmon nanoparticle region ($\lambda > 300$ nm). Most remarkably, a giant optical amplification from the DNA on Ag NCs is observed for the first time, with up to 85−103-fold enhance-ment per molecule relatively to free DNA with a native CD band at 240−280 nm. The observed CD signal is plasmon-induced, although plasmonic particles (NC) have no intrinsic CD signature. The observed "amplification" of CD signal is a consequence of the exciton−plasmon interaction within DNA-
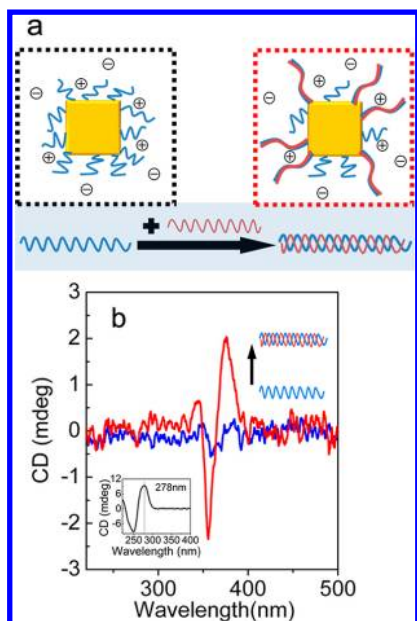
Figure 5. Recovery of plasmon-induced CD resonance in a salted solution after hybridization. (a) Scheme illustrating the change of conformation of DNA on a Ag cube surface in 0.1 M PBS: from flexible ssDNA (black-dotted frame) to rigid double helixes (red-dotted frame) when ssDNAs are hybridized with complementary strands. (b) The change of CD spectra from no signal (NC-ssDNA system, blue curve) to detectable CD signature (NC-dsDNA system, red curve) in 0.1 M PBS occurs after a complementary ssDNAs are hybridized with ssDNA attached to NC. The inset shows the native CD spectrum of free dsDNA in 20 μM concentration solution.

nanocube complex. Such a plasmon-induced CD resonance is sensitive to the molecular orientation with respect to a nanocube surface. A hybrid nanostructure and discovered phenomenon reported here would serve as a promising platform for ultrasensitive sensing of chiral molecules and their transformations in synthetic, biomedical, and pharmaceutical applications. Our approach also exhibits a great potential to realize an enhanced and tailorable optical response by combining various shaped nonchiral nanoparticle coupled with chiral molecular components. Such intrinsically nonchiral but optically chiral plasmonic elements might be utilized for optical nanomaterial. Furthermore, the new class of CD "amplifiers", shaped nanoparticles, calls for more comprehensive theoretical descriptions of the role of particle shapes for the plasmon-induced chiroptical activity. The future studies should address the relationship between chiral molecule, its placement and orientation, and nanoparticle geometry and its material on the plasmon-induced CD signal.

■ ASSOCIATED CONTENT

ⓢ **Supporting Information**

Materials and methods, numerical simulations discussion, and accompanying figures and tables. This material is available free of charge via the Internet at http://pubs.acs.org.

■ AUTHOR INFORMATION

Corresponding Author
*E-mail: ogang@bnl.gov.

Author Contributions
F.L. and Y.T. contributed equally.

■ REFERENCES

(1) Wagnière, G. H. *On chirality and the universal asymmetry: reflections on image and mirror image*; VHCA with Wiley-VCH: Zurich, 2007.

(2) Kadhane, U.; Holm, A. I. S.; Hoffmann, S. V.; Nielsen, S. B. *Phys. Rev. E* **2008**, 77, 021901.

(3) Fasman, G. D. *Circular dichroism and the conformational analysis of biomolecules*; Plenum Press: New York, 1996.

(4) Berova, N.; Woody, R. W.; Nakanishi, K. *Circular dichroism: principles and applications*, 2nd ed.; Wiley-VCH: New York, 2000.

(5) Barron, L. D. *Molecular light scattering and optical activity*, 2nd ed.; Cambridge University Press: Cambridge, 2004.

(6) Allenmark, S. *Chirality* **2003**, 15, 409.

(7) Ren, M. X.; Plum, E.; Xu, J. J.; Zheludev, N. I. *Nat. Commun.* **2012**, 3, 833.

(8) Helgert, C. *Nano Lett.* **2011**, 11, 4400.

(9) Guerrero-Martínez, A.; Auguié, B.; Alonso-Gómez, J. L.; Džolić, Z.; Gómez-Graña, S.; Žinić, M.; Cid, M. M.; Liz-Marzán, L. M. *Angew. Chem., Int. Ed.* **2011**, 50, 5499.

(10) Elliott, S. D.; Moloney, M. P.; Gun'ko, Y. K. *Nano Lett.* **2008**, 8, 2452.

(11) Hentschel, M.; Schaferling, M.; Weiss, T.; Liu, N.; Giessen, H. *Nano Lett.* **2012**, 12, 2542.

(12) Kuzyk, A.; Schreiber, R.; Fan, Z.; Pardatscher, G.; Roller, E.-M.; Högele, A.; Simmel, F. C.; Govorov, A. O.; Liedl, T. *Nature* **2012**, 483, 311.

(13) Moskovits, M. *Rev. Mod. Phys.* **1985**, 57, 783.

(14) Nie, S. M.; Emery, S. R. *Science* **1997**, 275, 1102.

(15) Lakowicz, J. R. *Anal. Biochem.* **2001**, 298, 1.

(16) Tan, S. J.; Campolongo, M. J.; Luo, D.; Cheng, W. L. *Nat. Nanotechnol.* **2011**, 6, 268.

(17) Govorov, A. O.; Fan, Z. Y.; Hernandez, P.; Slocik, J. M.; Naik, R. R. *Nano Lett.* **2010**, 10, 1374.

(18) Govorov, A. O. *J. Phys. Chem. C* **2011**, 115, 7914.

(19) Jeanmaire, D. L.; Vanduyne, R. P. *J. Electroanal. Chem.* **1977**, 84, 1.

(20) Slocik, J. M.; Govorov, A. O.; Naik, R. R. *Nano Lett.* **2011**, 11, 701.

(21) Hendry, E.; Carpy, T.; Johnston, J.; Popland, M.; Mikhaylovskiy, R. V.; Lapthorn, A. J.; Kelly, S. M.; Barron, L. D.; Gadegaard, N.; Kadodwala, M. *Nat. Nanotechnol.* **2010**, 5, 783.

(22) Gerard, V. A.; Gun'ko, Y. K.; Defrancq, E.; Govorov, A. O. *Chem. Commun.* **2011**, 47, 7383.

(23) Chen, W.; Bian, A.; Agarwal, A.; Liu, L.; Shen, H.; Wang, L.; Wu, C.; Kotov, N. A. *Nano Lett.* **2009**, 9, 2153.

(24) Lieberman, I.; Shemer, G.; Fried, T.; Kosower, E. M.; Markovich, G. *Angew. Chem., Int. Ed. Engl.* **2008**, 47, 4855.

(25) Mastroianni, A. J.; Claridge, S. A.; Alivisatos, A. P. *J. Am. Chem. Soc.* **2009**, 131, 8455.

(26) Hentschel, M.; Schaferling, M.; Weiss, T.; Liu, N.; Giessen, H. *Nano Lett.* **2012**, 12, 2542.

(27) Maoz, B. M.; Chaikin, Y.; Tesler, A. B.; Elli, O. B.; Fan, Z.; Govorov, A. O.; Markovich, G. *Nano Lett.* **2013**, 13, 1203.

(28) Guerrero-Martinez, A.; Alonso-Gomez, J. L.; Auguie, B.; Cid, M. M.; Liz-Marzan, L. M. *Nano Today* **2011**, 6, 381.

(29) Rycenga, M.; Cobley, C. M.; Zeng, J.; Li, W.; Moran, C. H.; Zhang, Q.; Qin, D.; Xia, Y. *Chem. Rev.* **2011**, 111, 3669.

(30) Zeng, J.; Zheng, Y.; Rycenga, M.; Tao, J.; Li, Z.-Y.; Zhang, Q.; Zhu, Y.; Xia, Y. *J. Am. Chem. Soc.* **2010**, *132*, 8552.

(31) Xia, X.; Zeng, J.; Zhang, Q.; Moran, C. H.; Xia, Y. *J. Phys. Chem. C* **2012**, *116*, 21647.

(32) Zhang, Q. A.; Li, W.; Moran, C.; Zeng, J.; Chen, J.; Wen, L.-P.; Xia, Y. *J. Am. Chem. Soc.* **2010**, *132*, 11372.

(33) Johnson, P. B.; Christy, R. W. *Phys. Rev. B* **1972**, *6*, 4370.

(34) McMahon, J. A.; Wang, Y.; Sherry, L. J.; Van Duyne, R. P.; Marks, L. D.; Gray, S. K.; Schatz, G. C. *J. Phys. Chem. C* **2009**, *113*, 2731.

(35) Govorov, A. O.; Fan, Z. Y. *ChemPhysChem* **2012**, *13*, 2551.

(36) Nykypanchuk, D.; Maye, M. M.; van der Lelie, D.; Gang, O. *Nature* **2008**, *451*, 549.

(37) Maye, M. M.; Nykypanchuk, D.; Cuisinier, M.; van der Lelie, D.; Gang, O. *Nat. Mater.* **2009**, *8*, 388.

(38) Sun, D. Z.; Gang, O. *J. Am. Chem. Soc.* **2011**, *133*, 5252.

(39) Jones, M. R.; Macfarlane, R. J.; Lee, B.; Zhang, J.; Young, K. L.; Senesi, A. J.; Mirkin, C. A. *Nat. Mater.* **2010**, *9*, 913.

(40) Artemyev, M.; Kisiel, D.; Abmiotko, S.; Antipina, M. N.; Khomutov, G. B.; Kislov, V. V.; Rakhnyanskaya, A. A. *J. Am. Chem. Soc.* **2004**, *126*, 10594.

(41) Cao, Y. W.; Jin, R.; Mirkin, C. A. *J. Am. Chem. Soc.* **2001**, *123*, 7961.

(42) Lee, J. S.; Lytton-Jean, A. K. R.; Hurst, S. J.; Mirkin, C. A. *Nano Lett.* **2007**, *7*, 2112.

(43) Lu, F.; Zhang, Y.; Zhang, L.; Zhang, Y.; Xang, J. X.; Adzic, R. R.; Stach, E. A.; Gang, O. *J. Am. Chem. Soc.* **2011**, *133*, 18074.

(44) Israels, R.; Leermakers, F. A. M.; Fleer, G. J.; Zhulina, E. B. *Macromolecules* **1994**, *27*, 3249.

(45) Ha, J. M.; Solovyov, A.; Katz, A. *Langmuir* **2009**, *25*, 10548.

(46) Hill, H. D.; Millstone, J. E.; Banholzer, M. J.; Mirkin, C. A. *ACS Nano* **2009**, *3*, 418.

(47) Zhulina, E. B.; Birshtein, T. M.; Borisov, O. V. *Eur. Phys. J. E* **2006**, *20*, 243.

(48) Flatau, P. J.; Draine, B. T. *Opt. Express* **2012**, *20*, 1247.

(49) Rivetti, C.; Walker, C.; Bustamante, C. *J. Mol. Biol.* **1998**, *280*, 41.

Discrete Nano-Cubes as Plasmonic Reporters of Molecular Chirality

Fang Lu[1], Ye Tian[1], Mingzhao Liu[1], Dong Su[1], Hui Zhang[2], Alexander O. Govorov[2]
and Oleg Gang[1*]

[1]Center for Functional Nanomaterials, Brookhaven National Laboratory

Upton, NY 11973, USA

[2]Department of Physics and Astronomy, Ohio University

Athens, Ohio 45701, USA

Materials and Methods

Au/Ag core-shell nanocube synthesis

Chemicals. Gold (III) chloride trihydrate ($HAuCl_4 \cdot 3H_2O$, 99.9+%), silver nitrate ($AgNO_3$, 99.9999%), sodium borohydrate ($NaBH_4$, 99.99%), L-ascorbic acid (AA, 99+%), cetyltrimethylammonium bromide (CTAB , 99.9%), and cetylpyridinium chloride (CPC, 99%) were purchased from Sigma-Adrich and used without further purification. Milli-Q water with a resistivity greater than $18.0M\Omega$ cm was used in the preparation of aqueous solutions.

Synthesis of Au octahedral seeds. The Au octahedral seeds were prepared using a two-step procedure (*1*). Firstly, 3nm Au nanoparticles were prepared by quickly injecting 0.60mL of ice-cold, freshly prepared $NaBH_4$ (10mM) into a rapidly stirred mixture of $HAuCl_4$ (10mM, 0.25mL) and CTAB (0.1M, 9.75mL). The resultant solution was stirred for 2 minutes and then left undisturbed for 2 hours. For the synthesis of CTAB-capped Au octahedral seeds, the formerly prepared hydrosol was diluted to 100mL with water, which was used as a seed solution. 0.1mL of 10mM $HAuCl_4$, 2mL of 0.2M CTAB, and 1.5mL of 0.1M AA were mixed together and the obtained colorless mixture was diluted to 25mL.And then 0.3mL of seed hydrosol was added to the mixture immediately. The reaction mixture was shaken enough, and then left undisturbed at room temperature for 8 hours. Finally, the mixture turned from colorless into light purple,

indicating the formation of Au nano-octahedra. The as-prepared products were collected by centrifugation (10min, 15000 rcf), washed with Milli-Q water once, and then re-dispersed into water with a same volume as reaction solution. The finally obtained solution was used as Au octahedral seeds.

Synthesis of Au/Ag core-shell nanocubes (NC). In a typical procedure, 10mL of the Au octahedral seeds and 1.6mL of 0.1M CPC aqueous solution were mixed in a 20mL vial. While the mixture was heated up to 60°C, 0.2mL of 10mM $AgNO_3$ and 0.8mL of 0.1M AA were added consecutively under magnetic stirring. After 1h reaction, the vial was cooled in an ice-bath. The as-synthesized nanoparticles were spun down (10min, 13400rcf) and re-suspended in deionized water (DIW) twice to remove excess surfactants and get concentrated suspension in DIW.

DNA functionalization of Au/Ag core-shell nanocubes

Thiol-modified single-strand oligonucletides (see Table S1 for sequences) were purchased from Integrated DNA Technologies Inc. with disulfide modification. Before nanoparticle DNA functionalization, the disulfide oligonucletides were first reduced by dissolving the lyophilized samples (100~300nmoles) in 0.3mL of a 100mM dithiothreitol (DTT) solution in purified water or buffer. The reduced DNA was loaded onto a freshly purified sephadex column (G-25, Amersham Bioscience) and eluted with 2.5mL of 10mM phosphate buffer (pH=7.4). The DNA was quantified using UV-Vis analysis using the known extinction coefficient.

Au/Ag core-shell nanocubes (NC) were functionalized with ssDNA (we have modifed a reported procedure(*2*)) using a ligand replacement reaction between CPC and thiol-modified oligonucletides for a high DNA coverage. Briefly, an aliquot of purified DNA solution was added to 1mL aliquot of freshly-dispersed NC (~2 OD_{260} of DNA for per mL of nanoparticle colloid). After allowing 3 hours for thiolated DNAs to react with the silver surface, particle suspensions were brought to 0.01% sodium dodecyl sulfate (SDS) and 10mM sodium phosphate and allowed to sit for overnight. Following literature procedure, the colloidal nanoparticle solutions were then slowly treated with NaCl to allow for electrostatic screening between neighboring DNA strands and denser surface coverage of oligonucleotides. Specifically, NaCl concentration of the solution was brought to 0.5M slowly by adding aliquots of 3M NaCl eight times with ~30mim interval for incubation. After reaching the final NaCl concentration, particles

were allowed to sit overnight to achieve maximum DNA loading. To remove the excess, unbound DNA from the solution, the mixture was centrifuged, the supernatant was removed, and the pellet was resuspended in washing buffer (0.01% SDS+10mM phosphate buffer, pH=7.4) three times. The final pellet was typically resuspended in 100µL to get a concentrated solution of particles. Sodium phosphate and NaCl were added to bring the final suspension to get expected concentrations of sodium phosphate and NaCl, respectively. The product concentration was quantified using the absorbance value at the surface plasmon resonance (SPR) maximum in UV-vis absorption spectra. A molar extinction coefficient of $\sim 5.5 \times 10^{10}$ $M^{-1} \cdot cm^{-1}$ at 452nm SPR peak is used for Au/Ag core-shell nanocubes with ~42nm edge length (see Fig. S6 and the corresponding description of calculations).

In order to get double helix DNA on the surfaces of Au/Ag nanocubes, the 30ssDNA-functionalized nanocubes were firstly hybridized by a 30 base ssDNA that is fully complementary to that grafted on nanocubes, at a molar ratio of 6000× in 0.2M PBS (*3*). This ratio is approximately a 10 fold excess of surface bound 30ssDNA when *n* of ~530 per nanocube is taken into account. The samples were incubated overnight to form dsDNA spacer segments and purified of excess un-hybridized complementary strands by multiple centrifugations and washing with buffer.

Synthesis and Functionalization of other nanoparticles used in the control experiments

Cubic and octahedral Au nanoparticles were synthesized by using the surfactant CPC according to the procedure developed by Niu *et al* (*4*). The spherical Au and Ag nanoparticles capped with the surfactant citrate were purchased from Ted Pella, Inc. These nanoparticles were functionalized with thiolated oligonucletides following the same protocol described above for Au/Ag core-shell nanocubes.

Sample Characterizations

Scanning electron microscope (SEM) and transmission electron microscope (TEM) characterizations were conducted on a Hitachi S-4800 Scanning Electron Microscope and a JEOL JEM-2100F high-resolution Analytical Transmission Electron Microscope, respectively.

Dynamic light scattering (DLS) measurements were preformed on a Malvern Zetasizer ZS instrument. UV-vis spectra were collected on a Perkin-Elmer Lambda 35 spectrometer. CD signals were recorded by the Jasco J-815 spectropolarimeter.

Quantization of DNA loaded on Ag nanocubes

A fluorescence-based method was used to determine the number of DNA loaded on cube and sphere surfaces (*5*). Firstly, the DNA was chemically displaced from nanoparticle surface using DTT. The displacement was initiated by adding equal volumes of DNA-functionalized nanoparticles and 1.0M DTT in 0.1M PBS, pH=7.4. The oligonucleotides were released into solution during overnight incubation, and the particle precipitate was removed by centrifugation. The concentrations of oligonucleotide in solution were determined by fluorescence spectroscopy. During the fluorescence measurement, the fluorophore was excited at 450nm and the emission was collected from 520 to 640nm.

Table S1. Nomenclature of oligonucleotide strands and sequences used in the study

Oligonucleotide	*Sequence*
30ss-DNA:	5'-SH- C_6H_{12}- $(T)_{15}$-TAA CCT AAC CTT CAT-3'
50ss-DNA:	5'-SH- C_6H_{12}-$(T)_{12}$- CGT TGG CTG GAT AGC TGT GTT CTT AAC CTA ACC TTC AT-3'
30ss-DNA-dye:	5'-SH- C_6H_{12}- $(T)_{15}$-TAA CCT AAC CTT CAT-Cy3-3'
Complementary DNA to 30ss-DNA:	5'-ATG AAG GTT AGG TTA-$(A)_{15}$-3'
30ds-DNA:	5'- TTT TTT TTT TTT TTT TAA CCT AAC CTT CAT-3' AAA AAA AAA AAA AAA ATT GGA TTG AAG TA

Table S2. Average Ag nanoparticle sizes, major SPR peak position, extinction coefficient at SPR peak α_{ext}, and the measured number of 30ssDNA strands on per particle for studied systems.

Nanoparticle	SPR peak position (nm)	Extinction coefficient α_{ext} (M^{-1}·cm^{-1})	DNA strands/particle
20nm-diameter Ag sphere	404	2.9×10^{9}	230±30
40nm-diameter Ag sphere	415	2.6×10^{10}	490±20
42nm-edge length Ag cube	452	5.5×10^{10}	530±40

Fig. S1
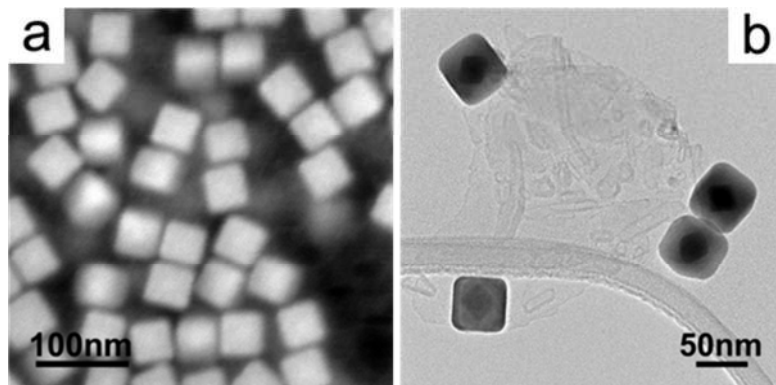
Figure S1: Representative electron microscope (EM) images of deposited nanocubes showing their two-dimensional projections. **a.** SEM. **b.** TEM. A gold-core octahedron is visible in the TEM image.

Fig. S2
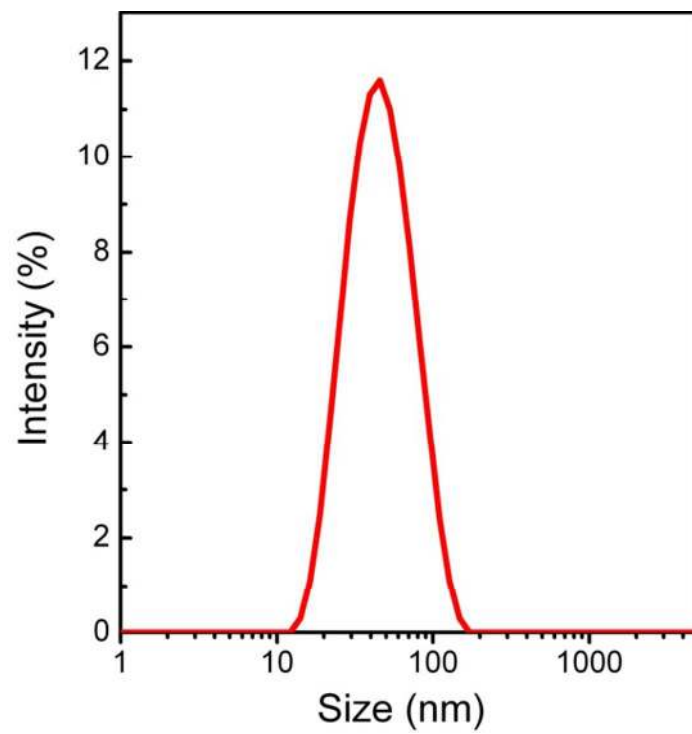
Figure S2: Dynamic light scattering (DLS) of ssDNA-functionalized Ag NCs.

Fig. S3

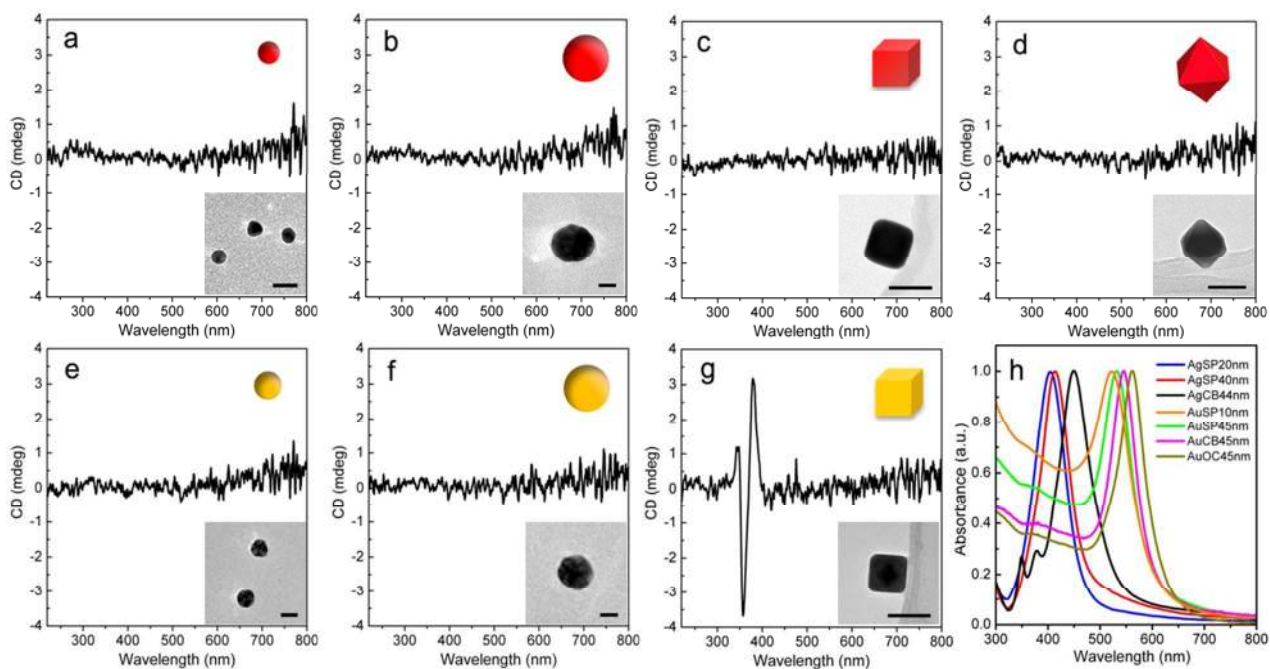**CD and UV-vis absorption spectra, TEM, and the corresponding shape cartoon images of other nanoparticles functionalized with DNA**

Figure S3: a-f. CD spectra, the representative TEM images and corresponding shape illustrations of 30ssDNA-functionalized nanoparticles: **a.** Au nano-spheres of 10nm in diameter (2nM); **b.** Au nano-spheres of 45nm in diameter (0.2nM); **c.** Au nano-cubes with edge length 45nm (0.2nM); **d.** Au nano-octahedra of 45nm in edge length (0.2nM); **e.** Ag nano-spheres of 20nm in diameter (1nM); **f.** Ag nano-spheres of 40nm in diameter (0.2nM). **g.** CD spectra, the representative TEM image and shape illustration of 50ssDNA-functionalized Ag NC with edge length 42nm (0.18nM). The corresponding CD signal is weaker than observed from 30ssDNA-functionalized Ag nanocubes, which is attributed to the lower coverage of NC with longer-chain DNAs. **h.** The normalized UV-vis absorption spectra of nanoparticles shown in **a-g**. Scale bars in the insets of **a, b, e, and f**: 20nm. Scale bars in the insets of **c, d, and g**: 50nm.
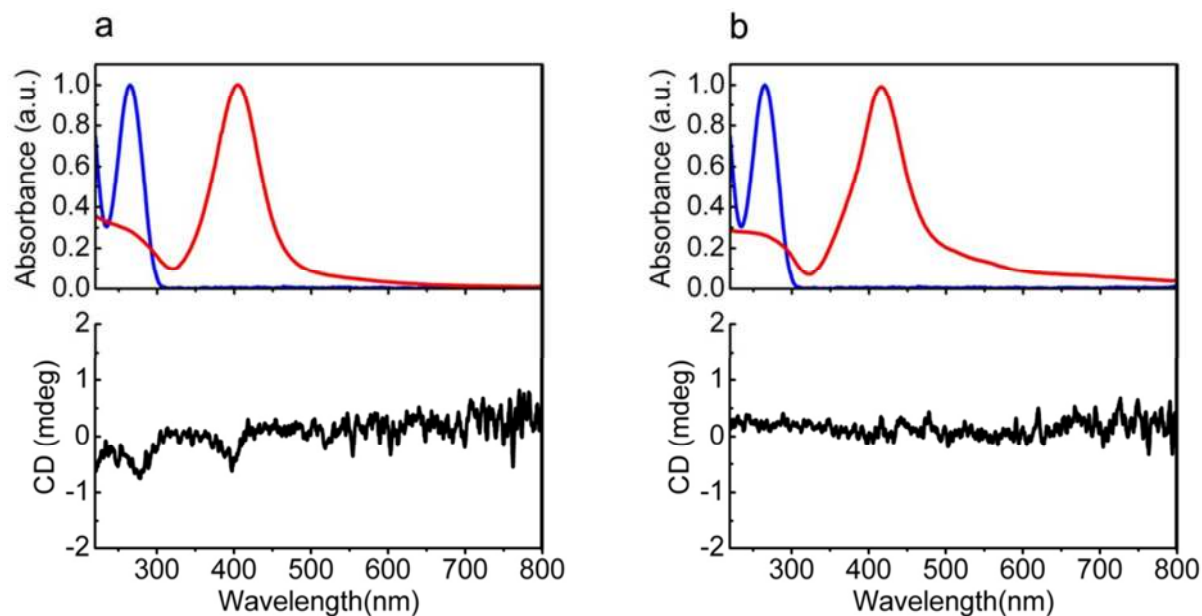
Fig. S4

Figure S4: a. (Upper) Normalized UV-Vis absorption spectra of 30ss-DNA (blue curve) and the 20nm Ag nanospheres functionalized with 30ss-DNA (red curve). The 30ss-DNA shows the characteristic UV peak at 264nm and the 20nm Ag nanospheres functionalized with 30ss-DNA show a surface plasmon resonance (SPR) peak at 404nm in the visible range, respectively. (Lower) CD spectrum of 20nm Ag nanospheres functionalized with 0.78 µM of 30ss-DNA (3.4nM of spheres) displays one negative peak at 277nm in the UV range and the other at 398nm in the visible range. An enhancement factor (A_{CD}) of 1.6 is estimated. **b.** (Upper) Normalized UV-Vis absorption spectra of 30ss-DNA (blue curve) and the 40nm Ag nanospheres functionalized with 0.196 µM of 30ss-DNA (0.4nM of spheres) (red curve). The 30ss-DNA functionalized 40nm Ag nanospheres show a SPR peak at 415nm in the UV-Vis spectrum (red curve, upper), but no signal in the CD spectrum (black curve, lower) is observed.

Numerical Simulations: the far-field and near-field optical properties of nanocubes

The far-field and near-field optical properties of the nanocubes are assessed by numerical simulation tools for two main purposes: 1) to obtain the optical extinction coefficient of the nanocube, which is critical for determining the mean DNA/nanocube ratio of the DNA-functionalized nanocubes; and 2) to evaluate the EM field enhancement in the vicinity of the nanocube for its SP resonance modes observed experimentally. For these simulations, the nanocube is idealized as a solid cube with edge D, and its edges and corners uniformly rounded with radius R (Figure S5). We define a dimensionless rounding factor $\beta = R/D$.

The far-field extinction spectrum of the nanocube is calculated using the finite-difference time-domain (FDTD) method to obtain its optical extinction coefficient. We choose the side width D = 42 nm and the round factor $\beta = 0.15$. We note that experimentally SEM/TEM observed β is around 0.1-0.2, although some rounding induced by electron beam cannot be excluded. For the best accuracy an octahedral gold core with 18-nm edge is placed at the center of the nanocube, with its diagonals coinciding with the four-fold axes of the cube. However, we do note that the simulated spectrum is not significantly altered even if we neglect the core/shell structure and simply treat the nanocube as solid silver NC. Due to the time-domain nature of the FDTD method, the strongly dispersive dielectric responses of gold and silver are modeled using the auxiliary differential equation (ADE) technique. Through this approach, the frequency-domain dielectric functions $\varepsilon(\omega)$ are expressed as the sums of Drude and Lorentzian terms, to account for the contributions from free electron absorption and interband transitions(6):

$$\varepsilon(\omega) = \varepsilon_\infty - \frac{\omega_D^2}{\omega^2 + i\gamma_D\omega} - \sum_{k=1}^{3} \frac{g_{L_k}\omega_{L_k}^2\Delta\varepsilon}{\omega^2 - \omega_{L_k}^2 + 2i\gamma_{L_k}\omega}.$$

The equation above is then fit to tabulated dielectric functions of gold and silver to obtain the parameters used for the simulation.(7, 8) The medium is modeled as a dielectric with a non-dispersive dielectric constant $\varepsilon = 1.77$ for water.

FDTD simulations are performed with a custom-developed code to obtain the optical scattering cross-section C_{sca} and absorption cross-section C_{abs} as functions of incident wavelength (Figure S6).(9) The extinction cross-section C_{ext} is calculated as their sum: $C_{ext} = C_{sca} + C_{abs}$. In the extinction spectrum we observe three plasmon modes including a primary feature at 450 nm (mode 1) and two smaller bands at 372 nm (mode 2) and 340 nm (mode 3) respectively, which closely matches the experimental spectrum shown in Figure 2a and 2c. We also obtain a close match for the peak width of the mode 1, which has an extinction cross-section $C_{ext} = 2.1$ x 10^4 nm^2 at the 450 nm peak. The peak extinction coefficient α_{ext} (450 nm) is therefore found at 5.5 x 10^{10} M^{-1}cm^{-1}, through the relation $\alpha_{ext} = C_{ext}N_A/\ln 10$.

Despite the close matches of peak positions obtained from the FDTD method, we note that the peak widths of the modes 2 and 3 are significantly exaggerated when compared to the experimental spectrum (Figure 2a), due to the difficulty for precisely modeling free electron relaxation over a broad spectral band, an intrinsic limit of the ADE technique. We then use the discrete dipole approximation (DDA), a frequency-domain method, to calculate the local field profile for the three modes, for which tabulated dielectric functions can be used. Using this approach we model our system, and close correspondence with the profile of the measured spectrum is obtained (Fig S7). Shown in Figure S7 is the extinction spectrum of a silver nanocube ($D = 42$ nm, $\beta = 0.05$) calculated by the DDA method, from which the three resonance modes are reproduced. Thus, the DDA allows us obtaining a 3D profile of the field enhancement for these three modes, as shown in the Figure 5. The local electric field enhancement of a few important reference points of NC, i.e. apexes (S8a), edges (S8b) and facets (S8c), and their spectral dependences are summarized in Figure S8.
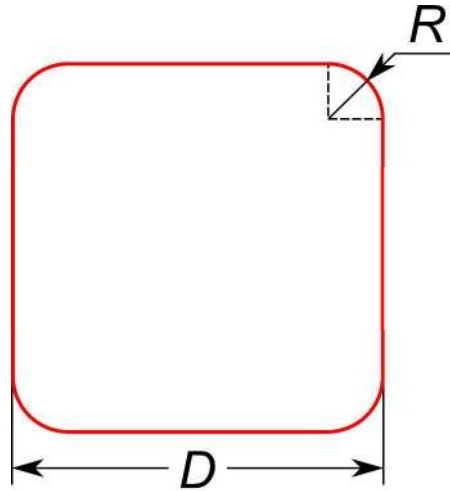
Fig. S5

Figure S5. Cross-section of the rounded cube used for the numerical modeling.
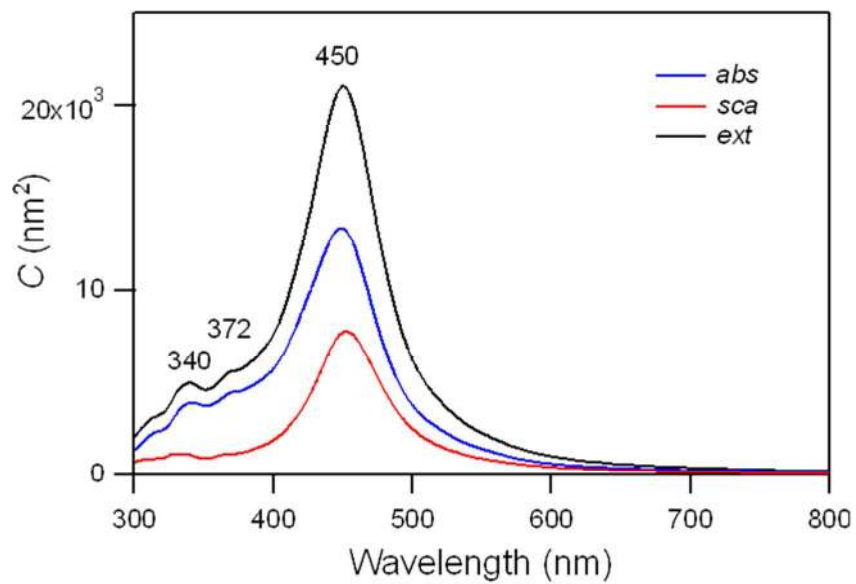
Fig. S6

Figure S6. FDTD-simulated optical absorption (blue), scattering (red), and extinction (black) spectra of a Au/Ag core/shell nanocube immersed in water.
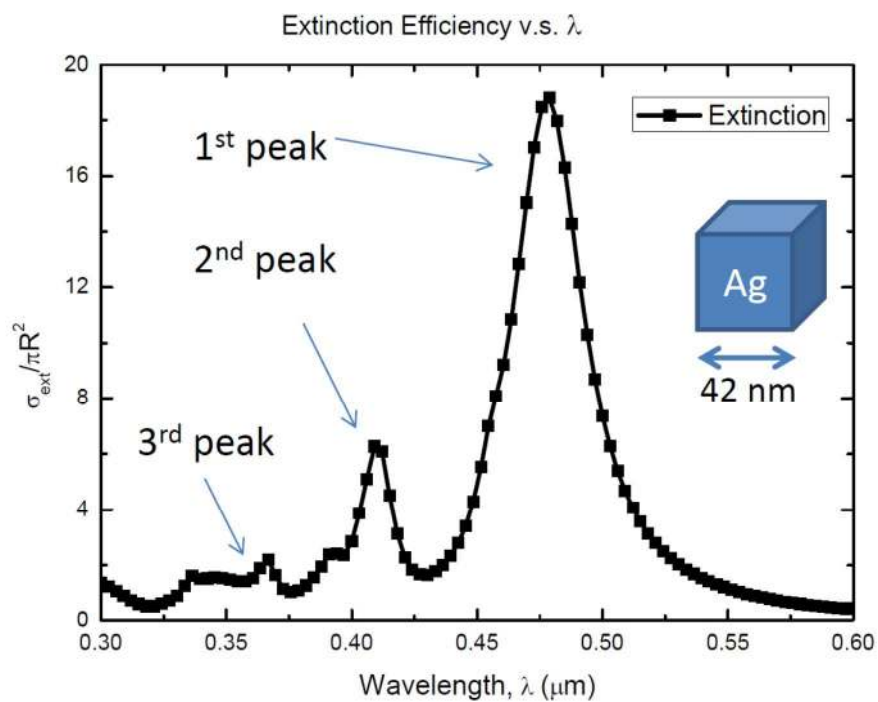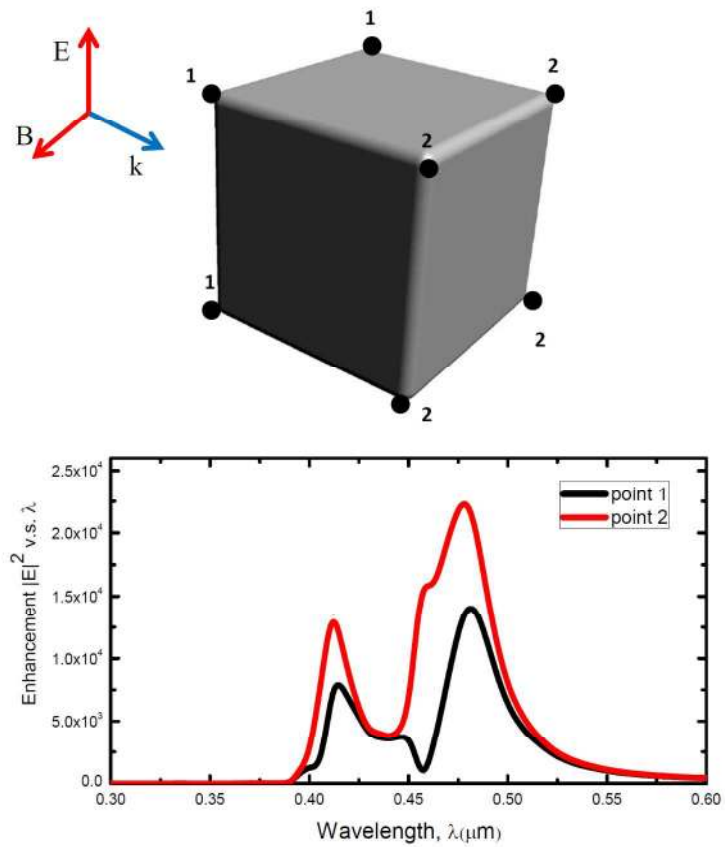
Fig. S7

Figure S7. Extinction spectrum of a cube calculated using the discrete dipole approximation (DDA) method 2 (*10, 11*), (*12*) and a local dielectric function taken from Ref. 7. The DDA code was taken from the open source at http://www.astro.princeton.edu/~draine/DDSCAT.html.
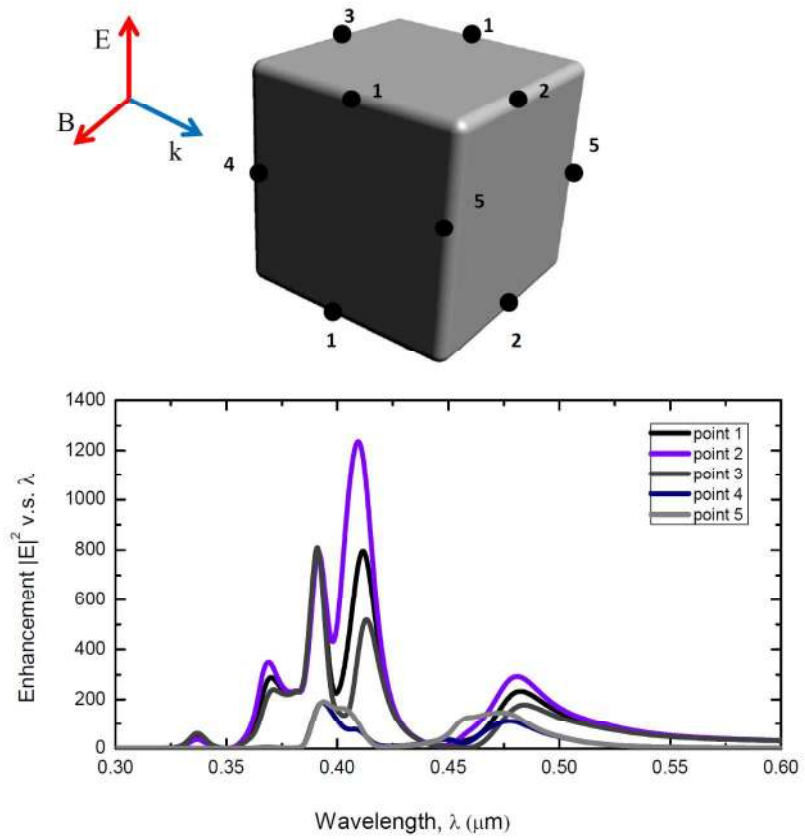
Fig. S8

Field-enhancement for the selected points on the Ag cube.
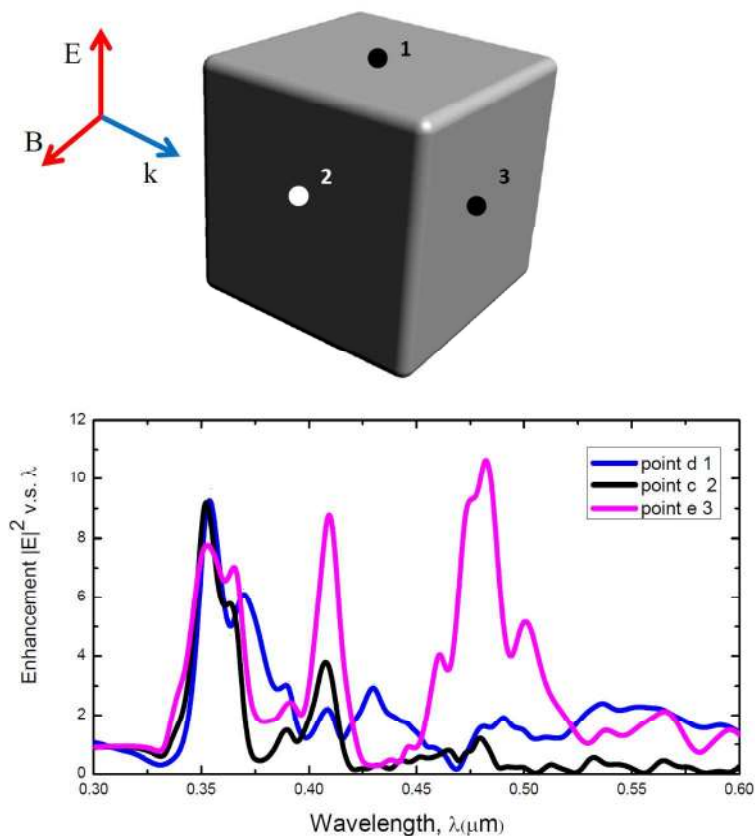
a

b

c

Figure S8. a. The calculated field enhancement ($P = |\vec{E}|^2 / |\vec{E}_0|^2$, where $|\vec{E}|$ and $|\vec{E}_0|$ are respectively the actual and incident electric field amplitudes, $|\vec{E}_0|=1$) at the apexes of the 42nm-silver cube. The main enhancement occurs for the main plasmon resonance (peak 1 in Fig. S7). **b.** The same for the edges. Interestingly, the main enhancement at the edges appears for the second and third resonances (Peaks 2 and 3 in Fig. S7). **c.** At the faces, the enhancement is relatively weak since the NC surface is smooth. Major enhancement effect is expected and then observed in our calculations at edges and apexes, where the metal surface has a high curvature.
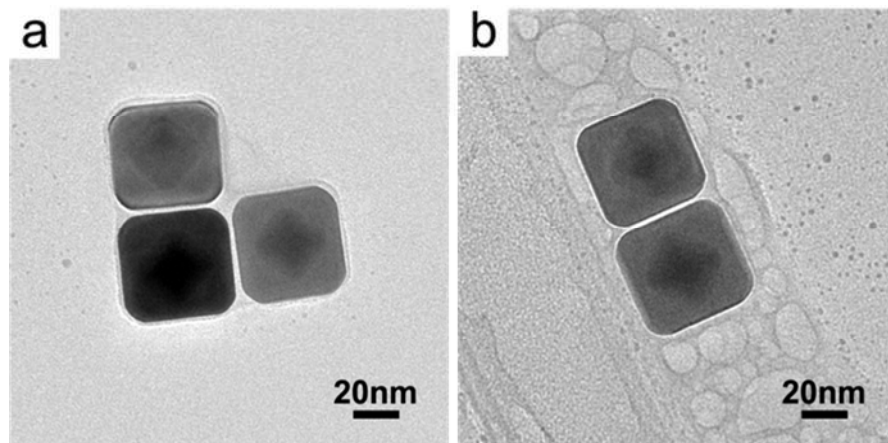
Fig. S9

Figure S9. TEM images of the DNA-functionalized Au/Ag core/shell nanocubes (**a**) before and (**b**) after stored in 0.5M PBS buffer (10 mM phosphate buffer, pH = 7.4, 0.5M NaCl) for 1h wherein no etching-induced damage is observed.

References

1. F. R. Fan *et al.*, *J Am Chem Soc* **130**, 6949 (Jun 4, 2008).
2. M. R. Jones *et al.*, *Nature Materials* **9**, 913 (Nov, 2010).
3. M. M. Maye, D. Nykypanchuk, D. van der Lelie, O. Gang, *J Am Chem Soc* **128**, 14020 (Nov 1, 2006).
4. W. X. Niu *et al.*, *Journal of the American Chemical Society* **131**, 697 (Jan 21, 2009).
5. S. J. Hurst, A. K. R. Lytton-Jean, C. A. Mirkin, *Anal Chem* **78**, 8313 (Dec 15, 2006).
6. A. Taflove, S. C. Hagness, *Computational electrodynamics : the finite-difference time-domain method*. Artech House antennas and propagation library (Artech House, Boston, ed. 2nd, 2000), pp. xxiii, 852 p.
7. E. D. Palik, *Handbook of optical constants of solids*. Academic Press handbook series (Academic Press, Orlando, 1985), pp. xviii, 804 p.
8. P. B. Johnson, R. W. Christy, *Phys Rev B* **6**, 4370 (1972).
9. M. Z. Liu, P. Guyot-Sionnest, T. W. Lee, S. K. Gray, *Phys Rev B* **76**, 235428 (Dec, 2007).
10. B. T. Draine, P. J. Flatau, *J Opt Soc Am A* **11**, 1491 (Apr, 1994).
11. P. J. Flatau, B. T. Draine, *Opt Express* **20**, 1247 (Jan 16, 2012).

12. Bruce T. Draine, Piotr J. Flatau, "User Guide to the Discrete Dipole Approximation Code DDSCAT 7.2" (2012) http://arxiv.org/abs/1202.3424